Laser-induced periodic surface structures: Fingerprints of light localization

J. Z. P. Skolski,[1,*] G. R. B. E. Römer,[2] J. V. Obona,[3] V. Ocelik,[3] A. J. Huis in 't Veld,[2,4] and J. Th. M. De Hosson[5]

[1]*Materials innovation institute M2i, Faculty of Engineering Technology, University of Twente, P.O. Box 217, 7500 AE, Enschede, The Netherlands*

[2]*University of Twente, Faculty of Engineering Technology, P.O. Box 217, 7500 AE, Enschede, The Netherlands*

[3]*Materials innovation institute M2i, Department of Applied Physics, University of Groningen, Nijenborgh 4, 9747 AG Groningen, The Netherlands*

[4]*TNO Technical Sciences; Mechatronics, Mechanics and Materials, De Rondom 1, 5600 HE, Eindhoven, The Netherlands*

[5]*University of Groningen, Department of Applied Physics, Materials Science Centre, Nijenborgh 4, 9747 AG Groningen, The Netherlands*

(Received 25 October 2011; revised manuscript received 1 February 2012; published 27 February 2012)

The finite-difference time-domain (FDTD) method is used to study the inhomogeneous absorption of linearly polarized laser radiation below a rough surface. The results are first analyzed in the frequency domain and compared to the efficacy factor theory of Sipe and coworkers. Both approaches show that the absorbed energy shows a periodic nature, not only in the direction orthogonal to the laser polarization, but also in the direction parallel to it. It is shown that the periodicity is not always close to the laser wavelength for the perpendicular direction. In the parallel direction, the periodicity is about $\lambda/\mathrm{Re}(\tilde{n})$, with $\tilde{n}$ being the complex refractive index of the medium. The space-domain FDTD results show a periodicity in the inhomogeneous energy absorption similar to the periodicity of the low- and high-spatial-frequency laser-induced periodic surface structures depending on the material's excitation.

DOI: 10.1103/PhysRevB.85.075320 PACS number(s): 42.25.Bs

I. INTRODUCTION

Laser-induced periodic surface structures (LIPSSs) were observed for the first time by Birnbaum in 1965.[1] The most common LIPSSs, also referred to as ripples, consist of wavy surfaces which can be produced on metals,[2,3] semiconductors,[4,5] and dielectrics.[6] When created with a linearly polarized laser radiation at normal incidence, these ripples have a periodicity close to the laser wavelength and a direction orthogonal to its polarization. Ripples having these properties can be produced with either cw lasers or pulsed lasers and are usually referred to as low spatial frequency LIPSSs (LSFLs). Ripples which are either orthogonal[7–15] or parallel[16–19] to the polarization, with a periodicity significantly smaller than the laser light, have been observed for laser pulse durations in the picosecond and femtosecond regime. These are often referred to as high spatial frequency LIPSSs (HSFLs), and as for LSFLs, they were observed on metals,[18,20] semiconductors,[7–12,16,17] and dielectrics as well.[13–15,19]

The influence of polarization, angle of incidence, and wavelength of a laser beam on LSFL formation strongly indicates that the phenomenon is mainly governed by the electromagnetic field. Emmony *et al.* suggested in 1973 that LSFLs were a consequence of interference between the incident laser beam and surface-scattered waves.[4] In 1983, Sipe *et al.* established a first-principles theory for LSFL formation, overcoming the physically inconsistent "surface-scattered wave" concept, by modeling the effect of surface roughness on the electromagnetic field.[21] The theory of Sipe *et al.*, also referred to as the *efficacy factor theory*, or *η theory*, in this article, was commonly accepted for the formation of LSFLs. The η theory is not only limited to ripples since it also predicts more complicated LIPSS patterns, usually investigated experimentally in the frequency domain using a diffraction setup.[5] As Clark *et al.* stated with respect to the η theory, it is "the most rigorous, comprehensive, and indeed the only (theory) that, to our knowledge, can accurately explain all of the observed LIPSSs."[22] Nevertheless the observation of new phenomena, such as HSFL formation, renewed interest in the topic since the early 2000s.

The origin of HSFL is still under debate and several theories have been proposed to explain their formation, such as self-organization,[13,16] second-harmonic generation,[7,8,12] or the η theory extended with a modification of the optical properties.[12,19,23] It must be noted that the η theory was created to explain LIPSS formation at a time when HSFLs had not yet been observed. However, the η theory predicts the presence of features which could explain the HSFLs parallel to the polarization.[12,19,23] HSFL is not the only phenomenon which renewed the interest in LIPSSs. For example, with the use of picosecond and femtosecond lasers, LSFLs with a periodicity smaller than the laser wavelength have been observed on different materials.[24] The objective of this article is to present results that are obtained numerically in order to overcome some limitations of the analytical approach of Sipe *et al.*

In this paper, the η theory and its limitations are first summarized. Second, the FDTD method is presented and is used to address some limitations of the η theory. Third, the results given by the FDTD method are shown in the frequency domain to allow comparison with the η theory. Finally, the space-domain results from the FDTD method are presented and discussed. Both of these approaches suggest that LIPSSs are a signature of the localization of light due to a rough surface.

II. LOCALIZATION OF LIGHT AND ROUGH SURFACES

A. Efficacy factor theory

The η theory predicts the inhomogeneous energy absorption of linearly polarized electromagnetic plane waves below a material's rough surface. The main assumption is that ripples grow where the absorbed energy is the largest.[21] The geometry

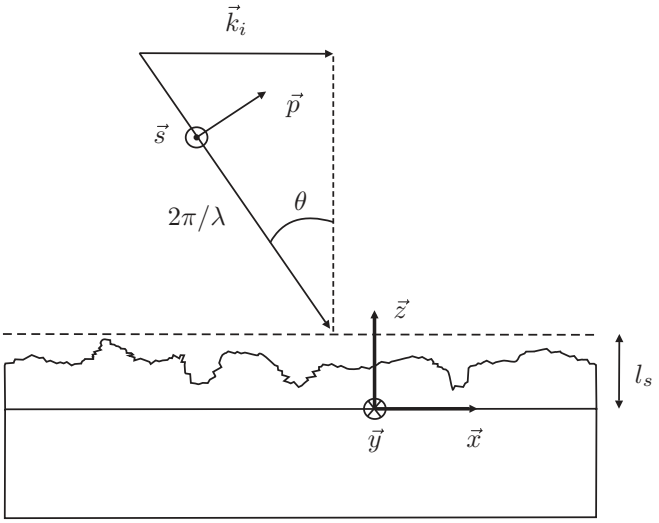

FIG. 1. Geometry and notations used in the η theory.

of the problem is shown in Fig. 1. For $z > 0$, there is vacuum. In a region of thickness l_s, referred to as the "selvedge," the surface roughness is confined. The region $z \leqslant 0$ is the bulk material. A plane wave of wavelength λ, $\vec{s}$ or $\vec{p}$ polarized, is incident on the selvedge region at an angle of incidence θ. The component of the wave vector parallel to the surface, the $(\vec{x},\vec{y})$ plane, is referred to as $\vec{k}_i$. The inhomogeneous energy absorption is studied in the frequency domain at $z = 0$, spanned by a vector $\vec{k} = (k_x,k_y)$ parallel to the surface and normalized by the norm of the wave vector, $2\pi/\lambda$. The η theory predicts

$$A(\vec{k}) \propto \eta(\vec{k},\vec{k}_i)|b(\vec{k})|, \tag{1}$$

where $A(\vec{k})$ is the inhomogeneous energy absorption at $z = 0$ in the frequency domain. The quantity $\eta(\vec{k},\vec{k}_i)$ is referred to as the *efficacy factor* and quantifies the efficacy with which the roughness leads to an inhomogeneous energy absorption at $\vec{k}$, while $b(\vec{k})$ is the Fourier component of the roughness. An expression for $\eta(\vec{k},\vec{k}_i)$ can be found in an article of Sipe *et al.*[21] For relation (1) to be valid, the thickness of the selvedge l_s must satisfy two inequalities. First, the selvedge thickness shall be small compared to the laser wavelength:

$$\frac{2\pi}{\lambda} l_s \ll 1. \tag{2}$$

Second, the selvedge thickness shall be small compared to the periodicity of the inhomogeneous energy absorption:

$$||\vec{k}||l_s \ll 1. \tag{3}$$

The surface roughness is described by a $b(x,y)$ binary function. That is, $b(x,y) = 0$ or 1 for the unfilled and filled parts of the selvedge, respectively. The efficacy factor is calculated for a random rough surface, $b(x,y)$ defined only statistically by the set (F,s). The quantity F, referred to as the *filling factor*, is the average of the $b(x,y)$ function. The quantity s, referred to as the *shape factor*, characterizes how the filled part agglomerates. It is comparable to half of the aspect ratio (the halfwidth divided by the height) of the filled parts of the selvedge. The best couple (F,s) found by Young

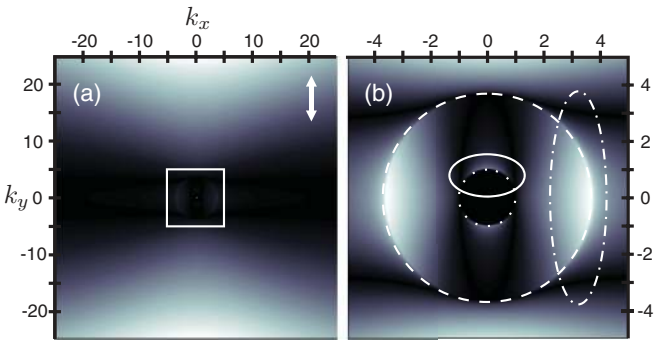

FIG. 2. (Color online) Two-dimensional (2D) η maps computed for $\theta = 0$, $\lambda = 800$ nm, $\tilde{n} = 3.692 + 0.065i$, and $(F,s) = (0.1,0.4)$. The polarization direction is indicated by the white arrow in (a). The white square in (a) indicates a zoom presented in (b). The solid and the dashed-dot ellipses enclose so-called type-s and type-d features, respectively. The dotted and dashed circles have radii $||\vec{k}|| = 1$ and $||\vec{k}|| = \mathrm{Re}(\tilde{n})$, respectively. A linear grayscale colormap is used, in which the brightest areas have the largest values.

et al. to describe LIPSSs equals (0.1,0.4), which corresponds to spherically shaped islands.[5]

An example of an η function for specific laser conditions impinging silicon, also referred to as an η map, is shown in Fig. 2. It is an η map corresponding to a beam at normal incidence $\theta = 0$ with a wavelength of $\lambda = 800$ nm, the optical properties of silicon at room temperature $\tilde{n} = 3.692 + 0.065i$,[25] a set $(F,s) = (0.1,0.4)$, and a polarization parallel to the y axis. In Fig. 2(a), only features for $k_y \geqslant 10$ are easily visible. The inequality (3) is not valid for these large values of k_y, therefore it is invalid to conclude anything concerning the influence of these features in the space domain. Moreover, their amplitude continues to increase with k_y, which is physically impossible. These features are referred to as type r in the rest of the article. In Fig. 2(b), two features can be observed: the one enclosed by the solid ellipse, referred to as type s,[5,23] and the feature enclosed by the dashed-dot ellipse, referred to as type d.[23] In this article, the "type-s" and "type-d" notations are used only for the frequency domain while the "LSFL" and "HSFL" notations are used in the space domain. For the sake of fluency, the word "features" may be omitted after "type s," "type d," and "type r." Since $\vec{k}$ is normalized by $2\pi/\lambda$, type-s features which follow the outer part of the $||\vec{k}|| = 1$ circle lead to a periodicity slightly smaller than λ in the space domain. The maxima of the type d are on the $||\vec{k}|| = \mathrm{Re}(\tilde{n})$ circle which correspond to a periodicity about $\lambda/\mathrm{Re}(\tilde{n})$ in the space domain. The type s and their behavior as a function of θ was extensively discussed in the past, since these features are responsible for the formation of LSFLs.[5] In comparison, type d have been rarely investigated.[12,19,23] The reason for this is that LIPSSs matching these periodicities have not been observed until the application of pico- and subpicosecond lasers.

The efficacy-factor theory has several drawbacks and some of them were already pointed out by its authors.[21] The transient changes of the material properties during a laser pulse, and the influence of the pulse duration itself, are not taken into account in the theory. This problem was partly solved by Dufft,[12] Bonse,[25–27] and their coworkers. They used a combination of

the Drude model with the η theory, also referred as to the Sipe-Drude model, to explain how the transient optical properties of ZnO and silicon can affect the LFSL characteristics. Several other aspects of LIPSS formation, such as the interpulse feedback mechanisms, remain unsolved in the η theory. Moreover, the inequalities (2) and (3) forbid an investigation of features present at large k_y and any possible dependence of the η maps with the depth z. The FDTD method is used in Sec. II C to study these latter two issues.

B. FDTD method

The FDTD method can be applied to numerically solve Maxwell's equations. It was introduced by Yee in 1966 and gained popularity with the increase of computational power.[28] Yee's algorithm is based on the two coupled Maxwell's curl equations. In the case of linear, isotropic, nondispersive materials, with no magnetic loss, Maxwell's curl equations can be written as[29]

$$\mu_0 \frac{\partial \vec{H}}{\partial t} = -\vec{\nabla} \times \vec{E}, \tag{4}$$

$$\epsilon_0 \epsilon_r \frac{\partial \vec{E}}{\partial t} + \sigma \vec{E} = \vec{\nabla} \times \vec{H}, \tag{5}$$

where t is the time, μ_0 is the free-space permeability, ϵ_0 is the free-space permittivity, ϵ_r is the relative permittivity, σ is the electric conductivity, $\vec{E}$ is the electric field, and $\vec{H}$ is the magnetic field. In Yee's algorithm, Eqs. (4) and (5) are expressed in a Cartesian frame. To numerically evaluate the equations, central differences are used for the finite-difference expressions of the space and time derivatives. The projection of the discretized Eq. (4) along the x axis is, for example,

$$\begin{aligned} H_x^{n+\frac{1}{2}}&\left(i,j+\frac{1}{2},k+\frac{1}{2}\right) \\ &= H_x^{n-\frac{1}{2}}\left(i,j+\frac{1}{2},k+\frac{1}{2}\right) - \frac{\Delta t}{\mu_0 \Delta y}\left[E_z^n\left(i,j+1,k+\frac{1}{2}\right)\right. \\ &\quad \left. - E_z^n\left(i,j,k+\frac{1}{2}\right)\right] + \frac{\Delta t}{\mu_0 \Delta z}\left[E_y^n\left(i,j+\frac{1}{2},k+1\right)\right. \\ &\quad \left. - E_y^n\left(i,j+\frac{1}{2},k\right)\right], \end{aligned}$$

where the superscript n indicates the time steps, Δt is the time increment, Δx, Δy, and Δz are the space increments, and i, j, and k are the discretized space coordinates.

One particularity of Yee's algorithm is that each component of $\vec{E}$ and $\vec{H}$ is respectively surrounded by four circulating components of $\vec{H}$ and $\vec{E}$, which makes the Yee mesh divergence-free. Such an arrangement, also referred to as Yee cell, is shown in Fig. 3. A so-called leapfrog arrangement is used for the time derivatives, meaning that each component of $\vec{H}$ is computed and stored using a previous $\vec{E}$, then all the $\vec{E}$ components are updated thanks to $\vec{H}$ and the cycle starts again. Apart from having to be chosen in adequacy with the considered problem, the Yee cell dimensions and the time increment shall be $\Delta t < \Delta t_{\max}$, with $\Delta t_{\max}$ equal to[29]

$$\Delta t_{\max} = c^{-1}\left(\frac{1}{\Delta x^2} + \frac{1}{\Delta y^2} + \frac{1}{\Delta z^2}\right)^{-\frac{1}{2}} \tag{6}$$

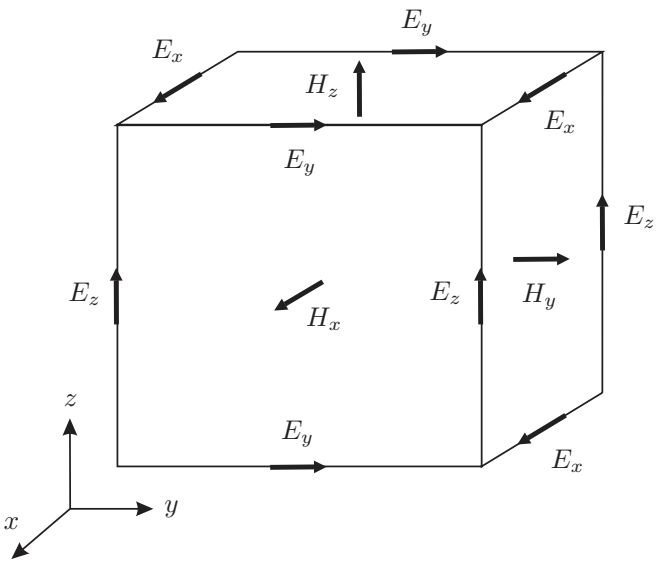

FIG. 3. Example of Yee cell. Each $\vec{H}$ component is surrounded by four circulating $\vec{E}$ components.

to ensure the algorithm's numerical stability. Here, c is the speed of light in vacuum.

In this article, the FDTD method is used to compute the inhomogeneous energy absorption below the material's surfaces. The geometry of the problem was already presented in Fig. 1. The study is performed for nonmetallic optical properties ($\epsilon_r > 0$) and at normal incidence of the laser light. The first limitation comes from the FDTD algorithm itself, which is not stable for metals without additional features. The second limitation allows us to keep the boundary conditions simple, while not significantly reducing the comparison with HSFLs produced in the literature. The simulation grid is terminated in the z direction by two so-called uniaxial perfectly matched layers (UPMLs), ten Yee cells wide to avoid nonphysical reflections.[30] In the x and y directions, periodic boundary conditions were used.[29]

To allow an easy comparison of FDTD results with the η theory, the geometry of Fig. 1 was followed for the simulation domain, as shown schematically in Fig. 4. The random roughness was introduced via the binary function $b(x,y)$, which indicates the filled and unfilled part of the selvedge, as described in Sec. II A. The *filling factor* F was set to 0.1 here while the *shape factor* s was taken into account by choosing carefully the volume occupied by one Yee cell and the number of layers describing the selvedge region. It is important to keep in mind that the Yee cell dimensions must be small compared to the laser wavelength and the studied phenomena. The Yee cell dimensions chosen were $\Delta x = 16$ nm, $\Delta y = 16$ nm, and $\Delta z = 5$ nm. With four layers describing the selvedge, the half aspect ratio of a filled area of the selvedge is equal to $\Delta x/(2 \times 4\Delta z) = 0.4$. With these parameters set, the roughness of the surface is comparable to the one described by the "best" couple $(F,s) = (0.1,0.4)$, discussed in Sec. II A. According to Young *et al.*,[5] "except for a factor independent of $\vec{k}$, in the case of s-polarized light, the (η) theory predicts no dependence of $\eta(\vec{k})$ on s and F." Hence,

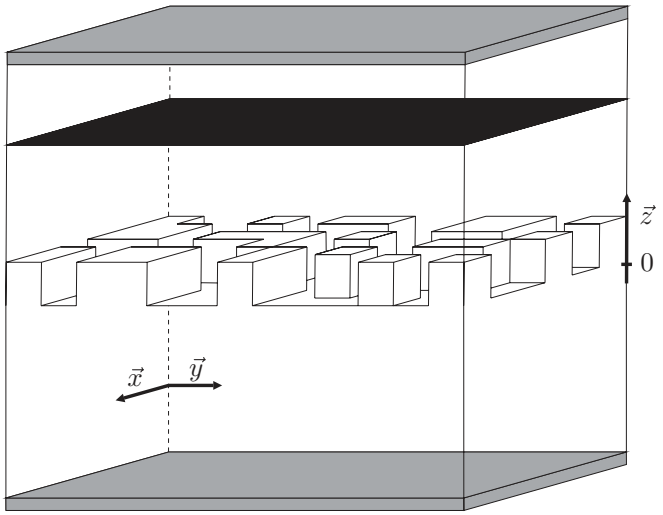

FIG. 4. Schematic of the simulation domain employed with the FDTD method. Note that the image is not to scale. The gray layers represent the UPML, while the black plane is the one from which the plane waves are sent.

the couple (F,s) is not critical for the features in the η maps at normal incidence.

The optical properties of the Yee cells follow the geometry of Fig. 1. That is, at $z \leqslant 0$ the optical properties of the Yee cells are set to that of the bulk material. For $0 < z \leqslant 4\Delta z$, the optical properties of the Yee cells are governed by the $b(x,y)$ function and, for $z > 4\Delta z$, there is vacuum. The number of Yell cells N_x in the x direction were chosen such that $N_x \Delta x$ is enough to resolve several wavelengths of the laser radiation λ. The same holds for N_y. More specifically, $N_x = N_y = 421$ were chosen, which implies a simulation domain larger than 8λ. The optical properties, ϵ_r and σ, were kept constant during the simulations. The number of Yee cells in the z direction N_z was set to 50. As mentioned in Sec. II B, the first ten and the last ten layers were occupied by the UPMLs (gray layers in Fig. 4). The thirtieth layer corresponds to $z = 0$. Hence, from the eleventh layer to the thirtieth layer, the inhomogeneous absorption can be studied up to 100 nm below the material's rough surfaces. The energy absorbed per wavelength below the selvedge was computed as the sum of the electric losses at each time step, $\sigma \Delta t ||\vec{E}||^2$, and was stored for each Yee cell. The time increment $\Delta t = 10^{-17}$ s satisfies inequality (6). The number N_t of time steps employed for a simulation depends on the optical properties of the considered medium and were chosen large enough to reach the steady state (constant energy absorbed per wavelength for each Yee cell). A two dimensional (2D) fast Fourier transform (FFT) was applied to the absorbed energy for (x,y) planes at different z locations in the bulk. Next, the results, referred to as FDTD-η maps, were compared to the η maps obtained. As in the η theory, only relative values were considered.

C. Comparison of η theory and FDTD simulation results

Figures 5(a) and 5(b) show FDTD-η maps at $z = 0$ nm for laser conditions comparable to the η maps presented in Fig. 2. FDTD-η maps are noisy compared to their counterpart. The reason is the FDTD method is used with a "real" roughness

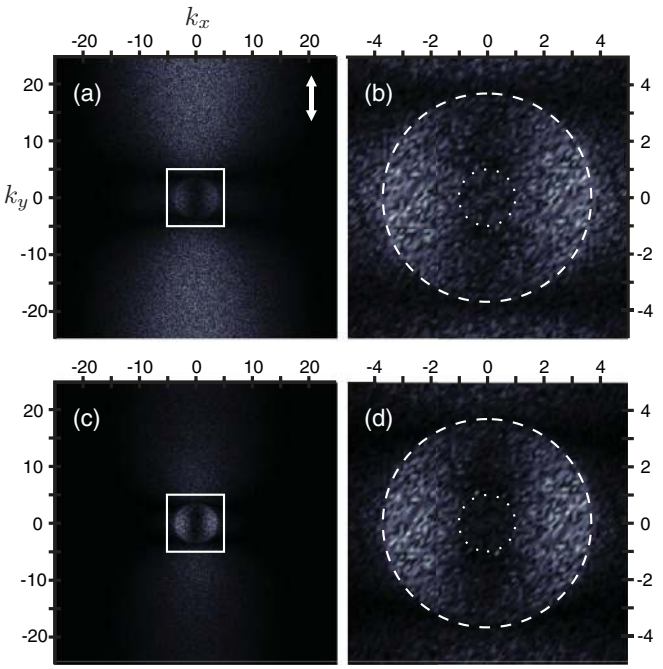

FIG. 5. (Color online) FDTD-η maps computed with $\theta = 0$, $\lambda = 800$ nm, $\tilde{n} = 3.692 + 0.065i$, $\Delta x = \Delta y = 16$ nm, $\Delta z = 5$ nm, $\Delta t = 0.01$ fs, $N_x = N_y = 421$, $N_z = 50$, and $N_t = 133295$. For (a) and (b) $z = 0$ nm and for (c) and (d) $z = -15$ nm. The polarization direction is indicated by the white arrow in (a). The white squares in (a) and (c) indicate zooms presented in (b) and (d), respectively. The dotted and dashed circles represent $||\vec{k}|| = 1$ and $||\vec{k}|| = \mathrm{Re}(\tilde{n})$, respectively. A linear grayscale colormap is used, the brightest areas have the largest values.

profile while an η map is an averaged solution.[21] The presence of the type-d features is confirmed by the FDTD-η maps, which means that ripples parallel to the laser polarization can be expected on materials showing suitable optical properties during the laser pulses. The shape and the position of the type d are in agreement with the η maps. However, the maximums of the type d are slightly shifted toward the inner part on the $||\vec{k}|| = \mathrm{Re}(\tilde{n})$ circle instead of being perfectly on the circle. In contrast to Fig. 2(a), type-r features are less spread and have bounded intensities. However, type-s features can be hardly observed for these chosen optical properties and this z location. Interestingly, for $z = -15$ nm and identical optical properties, the intensity of the type r is decreasing, while type-d features become the brightest and less spread, and type-s features start to be visible, as shown in Figs. 5(c) and 5(d). With increasing depth (not shown here), type-r features vanish and type-d features are more and more sharply defined. They loose progressively their extension outside the $||\vec{k}|| = \lambda/\mathrm{Re}(\tilde{n})$ circle while their maximum stays at the same position, close to the inner part of the circle. The designation "type r" was chosen because their appearance in the FDTD-η maps depends on the distance between the investigated (x,y) plane and the roughness layers. In other words, type-r features are strongly "roughness dependent."

The explanation of these differences between the FDTD-η and the η maps lies in the η theory approximations (2) and (3). Assuming l_s to be very small compared to λ in all the

calculations induces a loss of information for small depths, while the second inequality does not allow us to treat "high" values of $||\vec{k}||$ correctly. It must be noticed that the FDTD-η maps are based on the inhomogeneously absorbed energy while the η function is showing the efficacy with which the roughness leads to this inhomogeneous energy absorption. It is possible to calculate $\eta(\vec{k},\vec{k}_i)|b(\vec{k})|$, which is proportional to the inhomogeneous absorbed energy, for the same $b(x,y)$ function used by the FDTD method. However, this includes just "noise" on top of the shapes of the η function and none of the structure locations and general trends will be changed.

It is impractical to compare the results given by the η theory and the FDTD method for all λ, $\tilde{n}$, F, and s. Therefore, other comparisons presented in this section are carried out using the same approach as Bonse *et al.*, while testing the Sipe-Drude model.[25] That is, $\lambda = 800$ nm, $\theta = 0$, $F = 0.1$, and $s = 0.4$. The optical properties of the excited silicon are computed via the complex permittivity $\tilde{\epsilon}^* = \tilde{\epsilon} + \Delta\tilde{\epsilon}_{\text{Drude}}$ where $\Delta\tilde{\epsilon}_{\text{Drude}}$ is given by

$$\Delta\tilde{\epsilon}_{\text{Drude}} = \frac{-e^2 N_{\text{e}}}{\epsilon_0 m^*_{\text{opt}} m_{\text{e}} \omega^2 [1 + i(\omega\tau_{\text{D}})^{-1}]}. \quad (7)$$

where e, N_{e}, m^*_{opt}, m_{e}, ω, and τ_{D} are respectively the electron charge, the electron density in the conduction band, the optical effective mass of the carriers, the free electron mass, the angular frequency, and the Drude damping time. The values $m^*_{\text{opt}} = 0.18$ and $\tau_{\text{D}} = 1.1$ fs for femtosecond-laser-excited silicon were chosen in accordance with the article of Bonse *et al.*[25] The complex refractive index of the excited material $\tilde{n}^* = \sqrt{\tilde{\epsilon}^*}$ is used to compute the η maps while $\epsilon_r = \text{Re}(\tilde{\epsilon}^*)/\epsilon_0$ and $\sigma = \text{Im}(\tilde{\epsilon}^*)\omega$ are used for the FDTD-η maps.

Figure 6 shows the η maps and the FDTD-η maps for $N_e = 2 \times 10^{27}$ m^{-3} [Figs. 6(a) and 6(b)], $N_e = 3 \times 10^{27}$ m^{-3} [Figs. 6(c) and 6(d)], and $N_e = 4 \times 10^{27}$ m^{-3} [Figs. 6(e) and 6(f)]. The map for $N_e = 1 \times 10^{27}$ m^{-3} was omitted because it does not bring more information than the map for $N_e = 0$ m^{-3} nor for the map of $N_e = 2 \times 10^{27}$ m^{-3}. The FDTD-η maps are shown for $z = -15$ nm instead of $z = 0$ nm since it allows the best comparisons between the two approaches. The location and the relative intensities of the type-s and type-d features follow the same trends as in the η maps. As in the case of $N_e = 0$ m^{-3} [Fig. 5(d)], the maxima of the type d in the FDTD-η maps are slightly shifted toward the inner part of the $||\vec{k}|| = \text{Re}(\tilde{n})$ circle for $N_e \leqslant 3 \times 10^{27}$ m^{-3}, as shown in Figs. 6(b) and 6(d). In the η theory, the type r are unbounded for all N_e. Interestingly, the η and the FDTD-η maps behave similar to the type r for not-too-high $||\vec{k}||$. In the case where $N_e \leqslant 2 \times 10^{27}$ m^{-3}, the type-r structures never enter the $||\vec{k}|| = \text{Re}(\tilde{n})$ circles. Even if the type-s and type-r structures seem to merge in the case of $N_e = 3 \times 10^{27}$ m^{-3}, the type r vanish with increasing depths (not shown here). Regarding this, $N_e = 3 \times 10^{27}$ m^{-3} gives similar results as $N_e \leqslant 2 \times 10^{27}$ m^{-3}. The case where $N_e = 4 \times 10^{27}$ m^{-3} [Fig. 6(f)] is completely different: the type s and type r merge and going deeper does not change it. It is worth mentioning that, the higher the N_e, the slower the decrease of the type-r intensity with depth. Roughly, the type-r features lose almost completely their brightness at $z \approx 25$ nm for $N_e = 0$ m^{-3} and $z \approx 60$ nm for $N_e = 4 \times 10^{27}$ m^{-3}. Before disappearing, the type-r features evolve with the depth as follows: they lose their intensity, their spreading, and get progressively closer to the center. One last difference between the η and the FDTD-η maps is observed by comparing Figs. 6(e) and 6(f). The inner part of the $||\vec{k}|| = 1$ circles is always forbidden in the η maps, while the FDTD-η maps show the possibility to have an energy deposition with a periodicity larger than the wavelength of the laser light. The intensity of this energy deposition is slightly increasing with depth and with N_e, but remains small in comparison to the type s. Following these observations, one can expect LIPSSs with a periodicity above λ for higher excitation levels. It is important to notice that features, which are referred to as grooves, have been observed experimentally by Bonse and Krüger.[26] The grooves were found parallel to the polarization with a periodicity between approximately 1.9λ

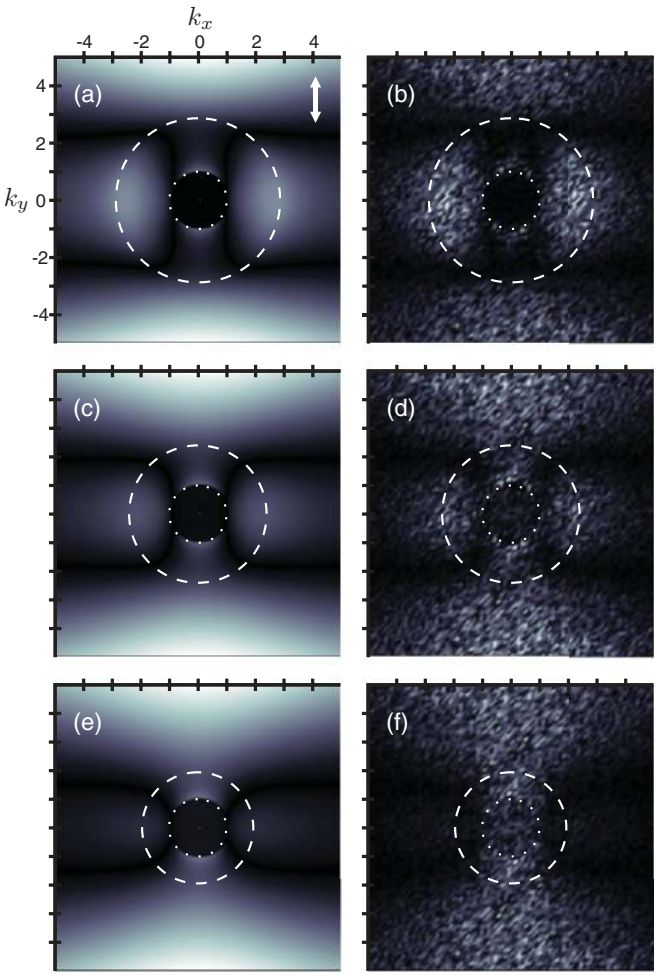

FIG. 6. (Color online) η and FDTD-η maps computed with $\theta = 0$, $\lambda = 800$ nm, and $(F,s) = (0.1,0.4)$. The FDTD-η maps are obtained with $\Delta x = \Delta y = 16$ nm, $\Delta z = 5$ nm, $\Delta t = 0.01$ fs, $N_x = N_y = 421$, $N_z = 50$, and $z = -15$ nm. For panels (a) and (b), $N_e = 2 \times 10^{27}$ m^{-3}, $N_t = 26794$, $\tilde{n}^* = 2.868 + 0.382i$. For panels (c) and (d), $N_e = 3 \times 10^{27}$ m^{-3}, $N_t = 13436$, and $\tilde{n}^* = 2.401 + 0.679i$. For panels (e) and (f), $N_e = 4 \times 10^{27}$ m^{-3}, $N_t = 13421$, and $\tilde{n}^* = 1.943 + 1.116i$. The polarization direction is indicated by the white arrow in (a). The dotted and dashed circles represent $||\vec{k}|| = 1$ and $||\vec{k}|| = \text{Re}(\tilde{n}^*)$, respectively. A linear grayscale colormap is used, the brightest areas have the largest values.

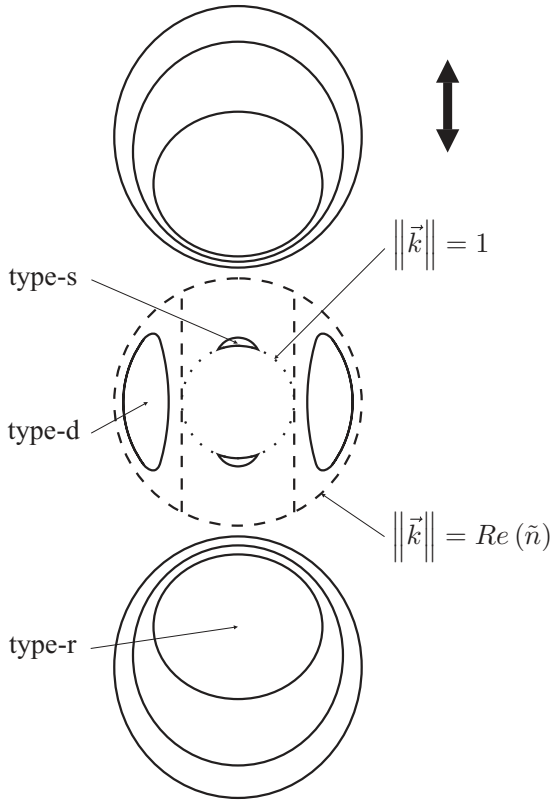

FIG. 7. Schematic representation of FDTD-η maps for $N_e \leqslant 3 \times 10^{27}$ m^{-3}. The polarization is indicated by the black arrow.

and 3.1λ. If an inhomogeneous energy absorption with such a periodicity would be present in the results of the simulation, the number of periods contained would be between 2.7 or 4.5. It means that the simulation domain is too small to study this phenomenon accurately. More simulations are required to confirm or invalidate the hypothesis that grooves can be explained with this approach. Nonetheless, the polarization dependence of grooves strongly suggest that, as for HSFL parallel to the polarization, this phenomenon is related to the inhomogeneous energy absorption below the material's rough surfaces.

Figure 7 shows a schematic representation of the FDTD-η map features for $N_e \leqslant 3 \times 10^{27}$ m^{-3}. To summarize, the type s follow the outer part of the $||\vec{k}|| = 1$ circle (dotted circle) which mean a periodicity slightly smaller than λ in the space domain. The type d follow the inner part of the $||\vec{k}|| = \mathrm{Re}(\tilde{n}^*)$ circle (dashed circle) leading to a periodicity of about $\lambda/\mathrm{Re}(\tilde{n}^*)$. The type r are confined to the $||\vec{k}|| > \mathrm{Re}(\tilde{n}^*)$ region. The relative intensity of the type s and type d is stable at $z \approx -15$ nm and the FDTD-η and the η maps are similar. The type r evolve from dominant at $z = 0$ nm to absent for higher depths, the evolution of their intensity depending on N_e. For the case where $N_e = 4 \times 10^{27}$ m^{-3}, it differs from Fig. 7. The type d are almost absent from the FDTD-η map, while the type r enter the $||\vec{k}|| = \mathrm{Re}(\tilde{n}^*)$ circle. This feature is discussed in more detail in the following part. The inner part of the $||\vec{k}|| = 1$ circle is not empty anymore.

III. SPACE-DOMAIN RESULTS

One of the advantages of the FDTD method, when studying LIPSSs formation, is its ability to study space-domain results. It allows us to determine which of the frequency domain features is dominant, while it is not always clear with the η theory. Figure 8 shows space-domain simulations of the absorbed energy per wavelength in an (x,y) plane for three different levels of excitation and two different depths below the material's rough surfaces. These pictures were obtained using the same simulation domain and conditions as in Sec. II C. As expected, the energy profile seems more "noisy" for $z = -25$ nm than for $z = -50$ nm. This is in agreement with the FDTD-η maps which shows stronger type r for lower depths. The lower level of excitation $N_e = 2 \times 10^{27}$ m^{-3} is characterized by an inhomogeneous energy absorption preferentially parallel to the polarization for both depths. It is actually the case for $N_e \leqslant 3 \times 10^{27}$ m^{-3} ($N_e = 0$ m^{-3} and $N_e = 1 \times 10^{27}$ m^{-3} are not shown here). However, one can notice that, for 50 nm depth, the energy absorption for $N_e = 3 \times 10^{27}$ m^{-3} [Fig. 8(b)] along the polarization direction is more regular than for $N_e = 2 \times 10^{27}$ m^{-3} [Fig. 8(d)]. This phenomenon is even more pronounced when N_e decreases. This observation seems in contradiction with the type d being brighter at lower N_e. While being indeed brighter, the type d occupy mainly the frequency region between $||\vec{k}|| = 1$ and $||\vec{k}|| = \mathrm{Re}(\tilde{n})$ (dotted curves in Fig. 7). Hence, they are more spread in the frequency domain, so less regular in the space domain.

The case where $N_e = 3 \times 10^{27}$ m^{-3} is particular, because it shows a competition between two directions in the inhomogeneous energy absorption. At $z = -50$ nm, the LIPSSs for $N_e = 3 \times 10^{27}$ m^{-3} looks like a transition state between $N_e = 2 \times 10^{27}$ m^{-3} with the absorption parallel to the polarization and the case for $N_e = 4 \times 10^{27}$ m^{-3} with a strong absorption in the perpendicular direction. Considering that ripples grow where the absorbed energy is the largest,[21] this switch of direction shows how important the type d are in the η theory. Moreover, it now seems possible to understand the existence of HSFLs in the silicon sample of Costache *et al.*[16] Costache observed a periodicity of $\Lambda_{\mathrm{HSFL}} \approx 200$ nm, which is close to the periodicity predicted in the $N_e = 0$ m^{-3} case $\Lambda_{\mathrm{HSFL}} = \lambda/\mathrm{Re}(\tilde{n}) = 217$ nm. The value of 200 nm, even if mentioned approximately, is low compared to the predictions. Especially, during a laser pulse, the silicon sample is inevitably excited and $N_e \gg 0$ which means that Λ_{HSFL} will more likely be between $\lambda/\mathrm{Re}(\tilde{n}) = 217$ nm and $\lambda/\mathrm{Re}(\tilde{n}^*(N_e = 3 \times 10^{27})) = 333$ nm. This first consideration is somewhat biased, though. The type d spread slightly outside the $||k|| = \mathrm{Re}(\tilde{n})$ circle for small depths, decreasing the periodicity of ripples in the space domain. This leads to an even more important consideration: neither the z location nor N_e are known since the method used suffers some of the problems of the Sipe-Drude model.[12,25–27] The electron density in the conduction band is assumed to be homogeneous and constant in the material. This is clearly not the case under ultrashort pulse processing because, even for $N_e = 0$ m^{-3}, the absorbed energy is inhomogeneous. Hence, N_e is neither homogeneous and varying in time as well. Other issues such as diffusion phenomena or the simple roughness model are affecting the energy absorption. Concerning the z

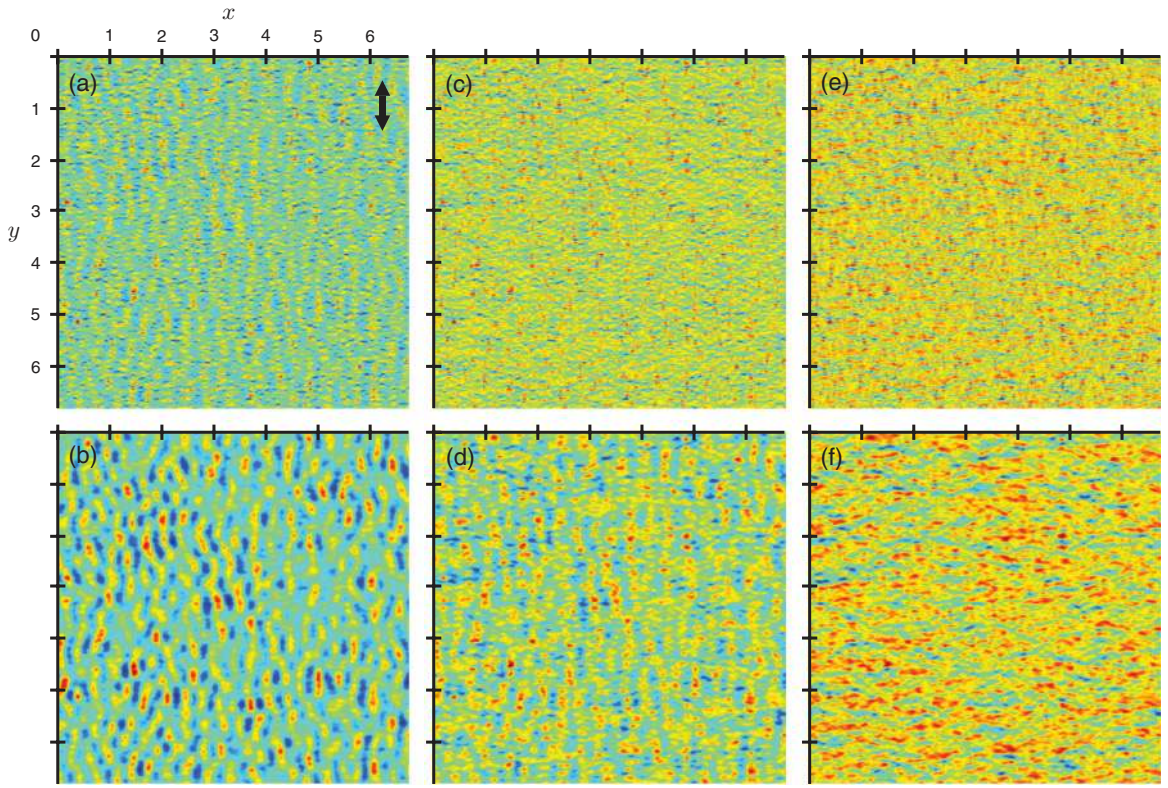

FIG. 8. (Color online) Results of FDTD simulations performed with the same parameters as in Fig. 6 for different depths and levels of excitation. For panels (a) and (b), $N_e = 2 \times 10^{27}$ m^{-3}; for panels (c) and (d), $N_e = 3 \times 10^{27}$ m^{-3}; and for panels (e) and (f), $N_e = 4 \times 10^{27}$ m^{-3}. For panels (a), (c), and (e), $z = -25$ nm; and for panels (b), (d), and (f), $z = -50$ nm. The polarization is indicated by the black arrow in (a). Each picture is shown with a colormap ranging from blue to red for the lowest to the highest value, respectively.

location, the melting and ablation processes should be modeled to know which thickness of the material surface is going to be removed and which part is molten and resolidified. Last but not least, the feedback mechanisms involved in LIPSS formation are not considered here. However, the simulations still provide qualitative predictions and an explanation for the existence of ripples parallel to the polarization. The fact that both type of ripples (perpendicular and parallel to the polarization) can be understood within a same theory makes it stronger. Moreover, when a silicon sample is machined with a Gaussian laser beam, HSFLs are supposed to be found in the outer part (low N_e) of the spot on the surface while LSFLs occupy the center if the fluence chosen allows them to coexist. This is also in agreement with the observations of Costache *et al.*[16]

Figures 8(e) and 8(f) show that, for the same level of excitation $N_e = 4 \times 10^{27}$ m^{-3}, but two different depths, the periodicity of the inhomogeneous absorbed energy can be different. This is again consistent with what was mentioned in part II C: the type s are not the only features contributing to the periodicity in the direction perpendicular to the polarization. The type r, which have a location, intensity, and spreading depending on the depth, are strongly influencing the periodicity seen in the space domain. This variation of periodicity with depth may explain the fact that LSFLs can have a periodicity much smaller than λ. The most recent theory involving electromagnetic waves to explain LSFL properties were mainly developed by Bonse *et al.* and Huang *et al.*[24–26] It is proposed that surface plasmon polaritons (SPPs) are responsible for the early-stage formation of LSFLs when the optical properties of the semiconductor reach the metallic state during femtosecond pulses. The excitation of SPPs is leading to have LSFLs with a periodicity smaller than λ. The fact that LSFL periodicity decreases with the number N of laser pulses applied is explained by a grating-assisted SPP mechanism, which triggers a redshift in the SPP resonance. The explanation involving SPPs in the early-stage formation of LSFLs seems consistent with the experimental results of Bonse *et al.* and Huang *et al.*[24–26] However, it is shown in Fig. 8(e) and 8(f) that an inhomogeneous energy deposition perpendicular to the polarization is possible without reaching metallic properties. Moreover, the SPP theory does not explain the switch of the LIPSS direction from parallel to perpendicular relative to the polarization, as observed by Costache *et al.*[16] It is proposed here that LSFLs can be produced with or without reaching the metallic state $\mathrm{Re}(\tilde{n}^*) < \mathrm{Im}(\tilde{n}^*)$.

Bonse and Krüger presented three different origins for the decrease of LSFL periodicity.[26] Two origins are not addressed in this article: the grating-assisted SPP mechanism mentioned above[24] and the change in the local angle of incidence.[8] The grating-assisted SPP mechanism is beyond the scope of this article because it involves a metallic state $\mathrm{Re}(\tilde{n}^*) < \mathrm{Im}(\tilde{n}^*)$ of the material as well as interpulse feedback mechanisms. The change in the local angle of incidence is not considered, since this study is performed at normal incidence of the laser light. The third origin for the decrease of LSFL periodicity, mentioned by Bonse and Krüger, concerns

the position and the width of the type-s features in the η maps as function of N_e.[25] It was shown that a variation of N_e, linked to a variation of fluence, can affect significantly the type-s features. Since the type s are considered to be responsible for the LSFL formation, a variation of fluence impacts the LSFL periodicity. As mentioned previously, the type-r features influence also the periodicity seen in the space domain in the direction perpendicular to the polarization. Hence, the variation of LSFL periodicity as a function of the fluence involves not only the type-s features, but also the type-r features. It is worth mentioning that, even if the $\mathrm{Re}(\tilde{n}^*) < \mathrm{Im}(\tilde{n}^*)$ range cannot be computed with the FDTD method employed, the η theory shows the presence of type-r features. Since, the η theory is limited by inequality (3), a conclusion is not allowed but one can expect an influence of the type-r features on LSFL periodicity even when metallic optical properties are reached. However, it is hard to determine how large the influence is of the type r on LSFL periodicity compared to the type s without considering interpulse feedback mechanisms.

IV. CONCLUSION

The FDTD method has been applied to study the inhomogeneous absorbed energy of linearly polarized laser radiation below a rough silicon surface. The numerical results, referred to as FDTD-η maps, show good agreement with the analytical solutions provided by the Sipe-Drude model. However, there are mainly three differences between the FDTD-η maps and the η maps. The first one concerns the type-r features, which are not described correctly by the η theory. These features are important because they modify the periodicity of the absorbed energy in the direction orthogonal to the polarization. The second difference is that the FDTD method allows calculations of the depth dependence of the FDTD-η maps, which was discussed in Sec. II C. The third difference is related to the $||\vec{k}|| < 1$ region of the frequency domain. While the η theory forbids the energy deposition with a periodicity larger than the wavelength of the laser light, the FDTD-η maps show that it is possible for sufficiently large N_e. Additional simulations are needed to know if the "grooves" observed by Bonse and Krüger can be understood in the frame of an electromagnetic approach.[26]

The study of the inhomogeneous absorbed energy in the space domain reveals that HSFLs parallel to the polarization can be expected at moderate excitation levels. Above a certain fluence threshold, LIPSSs with a periodicity perpendicular to the laser polarization should replace the HSFL parallel to the polarization. It was also proposed that LSFLs can be produced with or without reaching $\mathrm{Re}(\tilde{n}^*) < \mathrm{Im}(\tilde{n}^*)$ since the inhomogeneous energy absorption can be periodic in the direction perpendicular to the polarization without this inequality being satisfied. It is worth mentioning that the FDTD method can be used to study, at least qualitatively, the interpulse feedback mechanisms involved in LIPSS formation. Further work will be carried out in this direction.

ACKNOWLEDGMENTS

This research was carried out under project number M61.3.08300 in the framework of the Research Program of the Materials innovation institute M2i (www.m2i.nl).

*j.z.p.skolski@utwente.nl

[1] M. Birnbaum, J. Appl. Phys. **36**, 3688 (1965).
[2] M. Siegrist, G. Kaech, and F. Kneubühl, Appl. Phys. A **2**, 45 (1973).
[3] Y. Jee, M. F. Becker, and R. M. Walser, J. Opt. Soc. Am. B **5**, 648 (1988).
[4] D. C. Emmony, R. P. Howson, and L. J. Willis, Appl. Phys. Lett. **23**, 598 (1973).
[5] J. F. Young, J. S. Preston, H. M. van Driel, and J. E. Sipe, Phys. Rev. B **27**, 1155 (1983).
[6] P. Temple and M. Soileau, IEEE J. Quantum Electron. **17**, 2067 (1981).
[7] A. Borowiec and H. K. Haugen, Appl. Phys. Lett. **82**, 4462 (2003).
[8] J. Bonse, M. Munz, and H. Sturm, J. Appl. Phys. **97**, 013538 (2005).
[9] M. Couillard, A. Borowiec, H. K. Haugen, J. S. Preston, E. M. Griswold, and G. A. Botton, J. Appl. Phys. **101**, 033519 (2007).
[10] E. M. Hsu, T. H. R. Crawford, H. F. Tiedje, and H. K. Haugen, Appl. Phys. Lett. **91**, 111102 (2007).
[11] E. M. Hsu, T. H. R. Crawford, C. Maunders, G. A. Botton, and H. K. Haugen, Appl. Phys. Lett. **92**, 221112 (2008).
[12] D. Dufft, A. Rosenfeld, S. K. Das, R. Grunwald, and J. Bonse, J. Appl. Phys. **105**, 034908 (2009).
[13] J. Reif, F. Costache, M. Henyk, and S. V. Pandelov, Appl. Surf. Sci. **197–198**, 891 (2002).
[14] F. Costache, M. Henyk, and J. Reif, Appl. Surf. Sci. **208–209**, 486 (2003).
[15] M. Huang, F. L. Zhao, Y. Cheng, N. Xu, and Z. Xu, Phys. Rev. B **79**, 125436 (2009).
[16] F. Costache, S. Kouteva-Arguirova, and J. Reif, Appl. Phys. A **79**, 1429 (2004).
[17] T. Q. Jia, H. X. Chen, M. Huang, F. L. Zhao, J. R. Qiu, R. X. Li, Z. Z. Xu, X. K. He, J. Zhang, and H. Kuroda, Phys. Rev. B **72**, 125429 (2005).
[18] A. J. Huis in 't Veld and H. van der Veer, JLMN-Journal of Laser Micro/Nanoengineering **5**, 28 (2010).
[19] Q. Wu, Y. Ma, R. Fang, Y. Liao, Q. Yu, X. Chen, and K. Wang, Appl. Phys. Lett. **82**, 1703 (2003).
[20] A. Weck, T. H. R. Crawford, D. S. Wilkinson, H. K. Haugen, and J. S. Preston, Appl. Phys. A **89**, 1001 (2007).
[21] J. E. Sipe, J. F. Young, J. S. Preston, and H. M. van Driel, Phys. Rev. B **27**, 1141 (1983).
[22] S. E. Clark, N. C. Kerr, and D. C. Emmony, J. Phys. D: Appl. Phys. **22**, 527 (1989).
[23] J. Z. P. Skolski, G. R. B. E. Römer, A. J. Huis in 't Veld, V. S. Mitko, J. Vincenc Obona, V. Ocelik, and J. T. M. De Hosson, JLMN-Journal of Laser Micro/Nanoengineering **5**, 263 (2010).

[24]M. Huang, F. L. Zhao, Y. Cheng, N. Xu, and Z. Xu, ACS Nano **3**, 4062 (2009).
[25]J. Bonse, A. Rosenfeld, and J. Krüger, J. Appl. Phys. **106**, 104910 (2009).
[26]J. Bonse and J. Krüger, J. Appl. Phys. **108**, 034903 (2010).
[27]J. Bonse, A. Rosenfeld, and J. Krüger, Appl. Surf. Sci. **257**, 5420 (2011).
[28]K. S. Yee, IEEE Trans. Antennas Propag. **14**, 302 (1966).
[29]A. Taflove and S. C. Hagness, *Computational Electrodynamics: The Finite-Difference Time-Domain Method*, 3rd ed. (Artech House, Norwood, 2005).
[30]S. D. Gedney, IEEE Trans. Antennas Propag. **44**, 1630 (1996).